Environmental Science Nano

ROYAL SOCIETY OF CHEMISTRY

PAPER

View Article Online
View Journal

Cite this: DOI: 10.1039/d5en00836k

Linking protein corona composition to ecotoxicological outcomes: a comparative study of different engineered nanoparticles in Mediterranean sea urchin *Paracentrotus lividus*

Patrizia Romano, *[ab] Arianna Bellingeri, [a] Marco Morelli,[c] Rosanna Lucignano,[c] Eugenio Paccagnini,[d] Iole Venditti, [e] Andrea Carpentieri,[c] Pietro Lupetti,[d] Ilaria Corsi †[a] and Serena Leone †[b]

Once released into the environment, nanoparticles (NPs) rapidly interact with biomolecules present in biological fluids, leading to the formation of a protein corona that strongly influences their biological fate and interaction with living beings. In the field of ecotoxicology, investigating this bio–nano interface is crucial to understand how NPs are recognized and processed by marine organisms. In our study, we analyzed the formation of the protein corona around four NPs, two metal-based, AgcitLcys and TiO_2, and two polymer-based, PS-COOH and PS-NH_2, after incubation in the coelomic fluid (CF) of the sea urchin *Paracentrotus lividus*. NPs were characterized before and after incubation in CF using DLS and TEM, while proteomic analysis enabled the identification of adsorbed proteins and the estimation of their relative abundance. The composition of the coronas differed depending on the chemical nature and surface functionalization of the NPs, suggesting selective interactions with components of the CF biological matrix. *In vitro* bioassays on sea urchin's coelomocytes revealed distinct ecotoxicological outcomes among NPs: AgcitLcys induced the strongest effects, significantly reducing cell viability and lysosomal membrane stability at environmentally relevant concentrations (25 μg L^{-1}) while PS and TiO_2 elicited milder responses. A combined analysis of proteomic and *in vitro* data suggests that the protein corona is essential for mediating interactions between NPs and coelomocytes. The different affinity of NP surfaces for specific extracellular proteins may influence their recognition, internalization, and impact on cellular physiology. For instance, the corona formed around AgcitLcys contained proteins that bind to and transport other molecules, which could facilitate cellular interactions and activate redox and inflammatory pathways at the extracellular level, thereby modulating particles toxicity. Overall, our findings highlight the importance of accounting for the biological corona in the ecotoxicological assessment of NPs and confirm the protein corona as a key determinant in mediating nano–bio interactions in marine organisms.

Received 10th September 2025,
Accepted 6th April 2026

DOI: 10.1039/d5en00836k

rsc.li/es-nano

Environmental significance

To predict the fate and toxicity of nanoparticles (NPs) in marine ecosystems, it is essential to understand how they interact with extracellular proteins of biological fluids of marine organisms. This study investigated the protein coronas formed around four chemically distinct types of NPs in the coelomic fluid (CF) of *Paracentrotus lividus* and linked them to cellular effects. Our findings show how protein corona acts as a key molecular interface between NPs and cells, controlling how cells recognize, internalize, and react to them. These findings provide new insights into the mechanisms driving NP toxicity in marine invertebrates and into nanosafety assessment.

1. Introduction

In the nano-dimensional world, nanoparticles (NPs) never exist as isolated entities. Once suspended in environmental and/or biological fluids, their surfaces are in fact rapidly coated by a dense layer of proteins and other biomolecules, known as the protein corona.[1] This corona acts as a true "biological passport" for the NP and is composed of two

[a] *Department of Physical, Earth and Environmental Sciences, University of Siena, Italy. E-mail: patrizia.romano@student.unisi.it*
[b] *Department of Biology and Evolution of Marine Organisms (BEOM), Stazione Zoologica Anton Dohrn, Naples, Italy*
[c] *Department of Chemical Sciences, University of Naples "Federico II", Italy*
[d] *Department of Life Sciences, University of Siena, Italy*
[e] *Department of Sciences, Roma Tre University of Rome, Italy*
† These authors contributed equally and are listed alphabetically.

main layers: a hard corona, formed by high-affinity proteins that stably bind to the NP core and define its baseline identity over time; and a soft corona, consisting of lower-affinity proteins that dynamically exchange with the surrounding medium, flexibly regulating receptor recognition and the activation of cellular responses such as oxidative stress and/or immune signaling.[2]

In aquatic systems, protein adsorption dynamics play a crucial role in determining the behavior, bioavailability, and ecotoxicity of NPs released from widely used consumer products such as cosmetics, electronics, and wastewater treatment processes.[3–5] Metal-based and polymeric NPs have been increasingly detected in sediments and coastal waters near urbanized and industrial areas, suggesting chronic exposure for numerous marine species including benthic and filter-feeding organisms.[6,7] The widespread occurrence of NPs has prompted numerous studies investigating their biological effects on marine organisms. As Dedman *et al.*,[8] highlight, NPs toxicity is not solely determined by chemical composition. Instead, it results from a complex combination of physicochemical properties (*e.g.*, size, surface charge, and solubility), environmental transformations (*e.g.*, agglomeration and ion release), and interactions with dissolved biomolecules, particularly proteins. These interactions lead to the formation of a biomolecular corona that governs biological reactivity. Their review emphasizes the importance of considering species- and dose-specific effects across marine taxa, including diatoms, crustaceans, and bivalves, which are linked to oxidative stress, enzyme inhibition, and immune modulation. Brunelli *et al.*,[9] focus specifically on silver NPs (AgNPs), demonstrating how their high surface reactivity and ion release potential can induce adverse effects in microalgae, mussels, and fish. Major toxic mechanisms include mitochondrial dysfunction, redox imbalance, systemic inflammation, and gut microbiota alterations. The authors also underscore the role of biological matrices, especially the protein corona, in modulating NP uptake and cellular recognition. Feng *et al.*,[10] offer a complementary perspective, analyzing how corona composition influences NP fate, cellular targeting, and the potential co-transport of pollutants in marine systems. They demonstrate that the protein corona can dramatically alter the surface identity of NPs, enhance receptor-mediated interactions, and trigger redox and inflammatory responses. These effects are documented in various models, including sea urchins, tunicates, mussels, and crustaceans.[11] Altogether, these findings highlight that NPs released in marine waters are bioavailable and can interfere with key physiological processes across a wide range of taxa, although their effects vary depending on chemical nature, size, and exposure conditions. Within this context, the sea urchin *P. lividus* has emerged as an effective model organism for studying interactions between NPs and marine biological systems.[7,12–15] This species is widely distributed in Mediterranean coastal ecosystems, plays a key ecological role in benthic communities, and is commonly regarded as a sentinel species for environmental monitoring, due to its sensitivity to pollutants and well-characterized cellular and molecular responses.[16] Its coelomic fluid, rich in proteins and immune cells, provides a realistic biological matrix for examining protein corona formation and cellular-level responses under environmentally relevant conditions.[12,14] Several studies have demonstrated that NPs incubated in *P. lividus* coelomic fluid acquire specific protein coronas capable of modulating immune cell interactions.[17] Previous studies reported functional differences in the coronas formed on polymeric *versus* metallic NPs,[12,18] suggesting that coelomocytes respond in an active yet controlled manner to NPs, without signs of acute toxicity.[19–21] These findings confirm the suitability of *P. lividus* coelomic fluid and coelomocytes as a model system for investigating protein corona formation and the immuno-ecotoxicological outcomes in a marine species.

In this study, we adopted a holistic, integrated and multidisciplinary approach to investigate the formation and functional implications of protein coronas on four types of NPs differing in core chemical composition, size, and surface charge (Fig. 1). We selected two metal-based NPs (citrate and L-cysteine-coated silver NPs, namely AgcitLcys, and titanium dioxide, TiO_2) and two polystyrene based NPs (amino-functionalized, PS-NH_2, and carboxyl-functionalized, PS-COOH NPs). These NPs were selected for their broad relevance in industrial and biomedical applications and for their contrasting surface properties, which are expected to drive distinct bio–nano interactions. Unlike previous studies focused on individual particle types or limited endpoints, our approach combined the extensive physicochemical characterization of the four NP types and associated corona formation, using dynamic light scattering (DLS) and transmission electron microscopy (TEM), with an in-depth proteomic analysis of protein coronas formed upon contact with *P. lividus* sea urchin coelomic fluid (CF) by shotgun proteomics. To further explore the biological significance of corona formation, we conducted *in vitro* experiments, by directly exposing *P. lividus* coelomocytes to NPs in the presence of coelomic fluid as culture medium, thereby allowing protein corona formation to occur dynamically during cell–NP interaction. Under these conditions, we assessed three key ecotoxicological endpoints: cell viability, lysosomal membrane stability, and red cell amounts. This comprehensive strategy allowed us to identify the composition of the protein corona formed under controlled cell-free conditions and link its features to early immune cell responses, shedding light on NP bio–nano interactions in biologically relevant conditions. To our knowledge, this is the first study to systematically compare protein corona composition and immuno(eco)toxicological outcomes across both metal-based and polymer-based NPs in the same marine model organism, offering an important contribution to bridging this knowledge gap in marine nano-ecotoxicology.

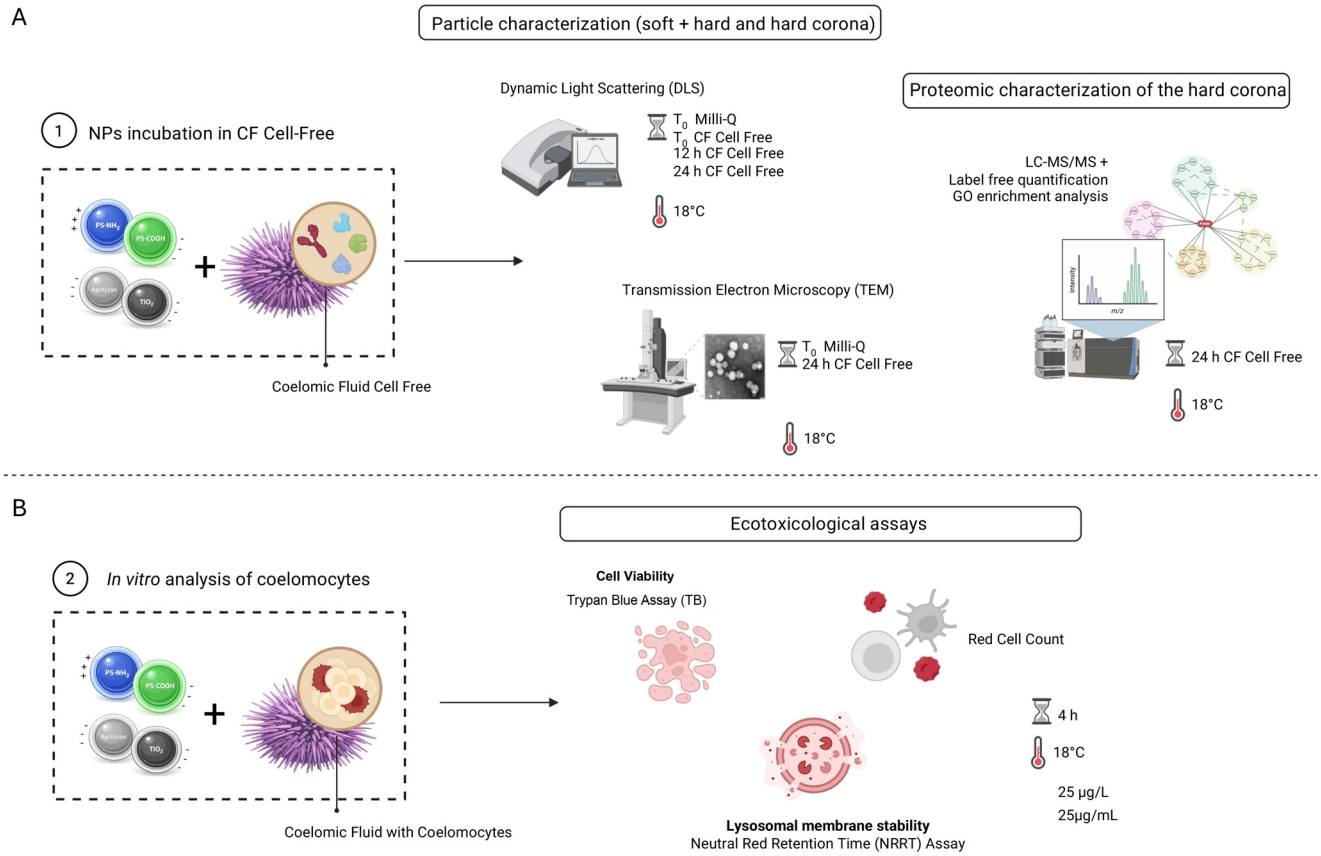

Fig. 1 Schematic overview of the experimental workflow divided into two sections. (A) NPs were incubated in cell-free CF to allow corona formation and subsequently characterized by DLS (T_0 – 24 h), TEM (24 h) and LC-MS/MS proteomics (hard corona, label-free quantification and GO enrichment). (B) NPs were exposed *in vitro* to coelomocytes (4 h; 25 µg L^{-1} and 25 µg mL^{-1}) and biological endpoints were assessed, including cell viability, red cell count, and lysosomal membrane stability. Created with https://BioRender.com.

2. Materials and methods

2.1 Animal collection and coelomic fluid preparation

Specimens of the Mediterranean sea urchin *P. lividus* (n = 15) with an average test diameter of 7 ± 0.5 cm were collected from two coastal sites in the Tyrrhenian Sea (Italy): Talamone (Grosseto, Tuscany) and the Gulf of Naples (Campania). Both locations are characterized by comparable Mediterranean environmental conditions and are not directly affected by anthropogenic disturbance. To minimize potential biological variability, sampling was performed exclusively during the winter season, a period preceding the main reproductive peaks of *P. lividus* and generally associated with more stable physiological conditions.[22–24] Only adult individuals of similar size were selected, including both males and females, to further reduce age- or reproductive stage-related variability.

After collection and prior to experimentation, sea urchins were maintained for 7 days under controlled laboratory conditions in filtered natural seawater (NSW; 0.45 µm; 18 ± 1 °C, salinity 38‰, pH 8). CF was withdrawn from each individual using a sterile syringe inserted into the peristomial membrane surrounding Aristotle's lantern and kept on ice. For each experimental phase, CF samples from all individuals were pooled to minimize inter-individual variability and to obtain a representative biological matrix, following an approach widely adopted in previous studies on *P. lividus*.[25,26] Each pooled CF preparation was centrifuged to remove coelomocytes, filtered (0.22 µm), aliquoted, and stored at −80 °C until use. Independent CF pools were prepared for protein corona characterization and as culture medium for the coelomocytes used in ecotoxicological studies.

2.2 Nanoparticles characterization

Unlabelled PS-NH_2 (50 nm, positively charged) and PS-COOH (60 nm, negatively charged) NPs were purchased in aqueous dispersion from Bangs Laboratories Inc., Fishers, IN. TiO_2 NPs (27 ± 2 nm) were provided by Degussa as Aeroxide® P25; AgcitLcys NP ($<R_H>$ = 8 ± 1 nm, size measured by DLS in Milli-Q using volume-based distribution to better represent primary particles) were prepared according to the procedure described by Prosposito *et al.*[27] The characterization of the four NP batches (PS-NH_2, PS-COOH, TiO_2 and AgcitLcys) in Milli-Q and CF was performed at a reference concentration of 50 mg L^{-1}. Prior to analysis, each NP suspension was sonicated in an ultrasonic bath (Mod. CP316, Ceia) for 10 s. The hydrodynamic diameter (D_H, nm) and ζ-potential (ζ_P,

mV) of the four NP dispersions were measured by dynamic light scattering (DLS) using a Zetasizer Nano ZS90 (Malvern) with the Zetasizer Software (version 7.02). These measurements were assessed at time zero (T_0) in Milli-Q and at T_0, 12 h and 24 h of incubation in the CF. Transmission electron microscopy (TEM) images of the four batches of NPs were obtained with a Tecnai G2 Spirit (FEI) in Milli-Q and in CF after 24 h of incubation. For TEM analysis, 3 μL of NP suspension were dropped onto Formvar-coated 300 mesh copper grids. After 2 minutes, excess liquid was blotted with filter paper, and the grids were air-dried or negatively stained with a 1% aqueous solution of uranyl acetate before observation in a Tecnai G2 Spirit (FEI) operating at an acceleration voltage of 120 kV. Particle size analysis was conducted by measuring the diameter of 100 particles using the FIJI ImageJ software. DLS and TEM measurements were conducted immediately after incubation in CF to characterize NPs with both a hard and a soft protein corona. In addition, to characterize NPs with the sole hard corona, measurements were repeated after three PBS washes performed by centrifugation (20 min, 18 000 × *g*, 18 °C) and followed by resuspension in Milli-Q.

2.3 Protein corona preparation and characterization

The four monodisperse NPs suspensions were incubated for 24 h at 18 °C in the dark using LoBind Eppendorf® tubes. The incubation was designed to promote the formation of a mature protein corona in the CF. We used the same number of particles per volume (50×10^{11} NPs mL^{-1}). After 24 h, NP–protein complexes were recovered following the protocol outlined by Monopoli *et al.*[28] The samples were centrifuged at 18 000 × *g* for 15 min at 18 °C and washed three times with phosphate-buffered saline (PBS) to remove the soft corona. The tightly bound protein fraction were then eluted with 50 μL of a protein solubilisation buffer (7 M urea, 2 M thiourea, 4% CHAPS and 1% DTT), sonicated in a bath for 15 min, and incubated at 25 °C for 15 min. These steps were repeated twice. A 10 μL aliquot of the supernatant containing the hard corona protein was used for analysis by SDS-PAGE and the remaining portion was stored at −20 °C to be later analysed by LC-MS (see below). Samples mixed with 2× reducing SDS sample buffer were heated for 5 min at 95 °C and loaded on 12% polyacrylamide gels. Gels were stained with Coomassie brilliant blue and imaged to visualize hard corona protein profiles.

The composition of the hard protein corona was characterized by LC-MS/MS using two aliquots from the same pooled CF sample as technical duplicates. Proteins were initially denatured by adding 50 μL of denaturing buffer (6 M urea, 25 mM NH_4HCO_3). Disulfide bonds were reduced by adding 20 μL of 100 mM dithiothreitol (DTT) in 50 mM NH_4HCO_3, followed by incubation at 60 °C for 1 h. Free thiol groups were subsequently alkylated by adding 20 μL of 120 mM iodoacetamide (IAM) in 50 mM NH_4HCO_3, and the reaction was carried out in the dark for 1 h. A second reduction step was then performed by adding 20 μL of 100 mM DTT in 50 mM NH_4HCO_3, with incubation for 1 h at room temperature. Samples were diluted with 50 mM NH_4HCO_3 to reduce the urea concentration to 1 M, and proteins were digested by adding 4 μL of trypsin solution (1 μg μL^{-1} in 10 mM NH_4HCO_3). Enzymatic hydrolysis was carried out for 16 h at 37 °C and subsequently stopped by adding 10% formic acid. Samples were centrifuged at 10 000 rpm for 10 min and dried using a Savant concentrator. Peptide mixtures were analyzed using an LTQ Orbitrap XL™ Hybrid Ion Trap-Orbitrap mass spectrometer (Thermo Fisher Scientific, Bremen, Germany), as previously described.[29] Raw data files were processed with PeaksX PRO software,[30] which enables *de novo* assisted protein identification. As a reference database, we used the translation of the protein coding sequences from the recently published genome of the sea urchin *P. lividus*.[31] The predicted proteome was annotated with InterProScan.[32] Functional enrichment analyses were performed in R using the topGO package,[33] employing as background the combined proteome detected across all four NP types. To enable relative protein quantification within each NP batch, normalized spectral abundance factors (NSAF) were calculated from spectral counts across samples.[34] Principal component analysis (PCA) was performed on NSAF values using R's prcomp function with scaling.

2.4 Cultures of *P. lividus* coelomocytes for ecotoxicological studies

In vitro cultures of coelomocytes from the sea urchin *P. lividus* were obtained following published protocols.[14,35] CF, used as an exposure medium, was collected as previously described using a 1 mL sterile syringe preloaded with CMFSW-EH anticoagulant solution (calcium- and magnesium-free seawater with EDTA and HEPES) in a 1 : 1 ratio to prevent clotting (NaCl 460 mM; KCl 10.7 mM; EDTA 70 mM; HEPES 20 mM; Na_2SO_4 7 mM; $NaHCO_3$ 2.4 mM, pH 7.4), following the procedure of Smith's protocol.[36] The cell suspension was obtained by centrifuging the CF at 600 × *g* for 20 minutes at 4 °C, followed by resuspension in 0.22 μm filtered CF. The composition of the heterogeneous population of coelomocytes (phagocytes, vibratile cells, red and white amoebocytes) was observed prior to exposure to NPs, based on the work of Pinsino and Matranga,[37] using a Luna II automated cell counter (Logos Biosystems Inc., see SI for instrument settings) and confirmed by light microscopy using a FastRead® 102 camera. Coelomocytes suspensions in CF at a density of 1×10^6 cells per mL in 24-well plates were incubated in the dark at 18 °C for up to 4 h with the four batches of NPs at concentrations of 25 μg L^{-1} and 25 mg L^{-1}. The two concentrations tested were chosen as acute and more realistic exposure levels based on predicted environmental concentration (PEC) for marine coastal areas as already described.[14,16] Exposure concentrations in all *in vitro* assays

were expressed on a mass basis (μg L^{-1} and mg L^{-1}), following standard ecotoxicological analysis. Theoretical particle number and total surface area corresponding to these concentrations were estimated for each NP type and are reported in SI (SI1 Table S5). All experiments were conducted in triplicate. Data are presented as mean ± SD. Statistical comparisons were performed using a non-parametric Kruskal–Wallis test followed by Dunn's *post hoc* multiple-comparisons test; significance levels are indicated as $*p < 0.05$, $**p < 0.01$, $***p < 0.001$, $****p < 0.0001$.

2.5 Cell viability

To assess coelomocytes viability we used the trypan blue exclusion assay following the protocol by Strober *et al.*[38] At the end of the 4 h of exposure, coelomocytes were centrifuged at 600 × *g* for 10 minutes at 4 °C, and then incubated with 0.4% trypan blue in 1× PBS for 4 minutes. Following incubation, the cells were transferred onto slides and examined using an optical light microscope (Olympus BX51, Tokyo, Japan). The percentage of viable cells was determined by counting the number of viable cells per 100 coelomocytes.

2.6 Lysosomal membrane stability

The neutral red retention time (NRRT) assay according to the method by Lowe *et al.*,[39] was adapted following the protocol by Marques-Santos *et al.*[14] At the end of 4 h of exposure, 200 μL of coelomocyte suspensions were placed on a 22 × 22 mm coverslip and left in a humidified chamber at 18 °C for 1 h in the dark. Then, cells were incubated for 30 minutes at 18 °C with 200 μL of NR dye solution (final concentration of 40 μg mL^{-1}, prepared from a 40 mg mL^{-1} NR stock solution in DMSO). Excess dye was removed by washing with a buffer solution (20 mM HEPES; 436 mM NaCl; 53 mM $MgSO_4$; 12 mM KCl; 12 mM $CaCl_2$, pH 7.5), and the coverslips were mounted on slides and sealed. The slides were then examined every 15 minutes under an optical light microscope (40×, Olympus BX51, Tokyo, Japan), and the percentage of cells exhibiting NR dye leakage into the cytosol was recorded. At each time point, an average of 100 cells was analyzed, with the endpoint defined when 50% of the cells showed lysosomal leakage, indicated by red-stained cytosol and rounded cell morphology. The assay was conducted in triplicate and repeated three times.

2.7 Red cell

At the end of 4 h of exposure, 100 μL of cell suspension was placed on a slide and incubated for 1 h in a humid chamber at 18 °C in the dark. After removing excess cells, the slide was checked under an optical microscope (40×, Olympus BX51, Tokyo, Japan) and the number of red amoeboids out of 100 immune cells was counted, without the use of any staining procedure as they are readily distinguishable thanks to their intrinsic pigmentation.

3. Results

3.1 Particle characterization

The behavior of the four types of NPs in Milli-Q and CF investigated using DLS and TEM is shown in Fig. 1 and 2 and in Tables S1–S4. DLS profiles were recorded after incubation at three different time points (T_0, 12 h, and 24 h) to monitor the dynamic evolution of the protein corona and characterize NPs bearing either a soft and hard corona or only the hard corona. TEM images were acquired at T_0 in Milli-Q and at 24 h of incubation in the CF, to provide ultrastructural confirmation and dimensional measurements of corona formation.

PS-NH_2 and PS-COOH NPs appeared as monodisperse suspensions in Milli-Q (Fig. 1A and B; Tables S1 and S2), with average D_H of 63.2 ± 1.3 and 81.0 ± 1.1 nm, respectively. Both PS-based NPs displayed charged surfaces, as shown by the ζ_P of +47.2 ± 1.3 mV (PS-NH_2) and −39.6 ± 0.91 mV (PS-COOH), respectively indicating a strong electrostatic stabilization provided by surface functionalization.[1] AgcitLcys NPs (Fig. 1C; Table S3) showed a broader size distribution centered around 56.8 ± 2.3 nm when measured in intensity mode, reflecting the contribution of larger aggregates, and a strongly negative ζ_P (−51.8 ± 0.7 mV). This is consistent with the presence of deprotonated carboxylate and thiol groups on the particle surface, derived from the citrate and L-cysteine coating suggesting also a moderate colloidal stability primarily driven by electrostatic repulsion, in agreement with previous studies.[40,41] In contrast, TiO_2 NPs formed large agglomerates in Milli-Q (Fig. 2D; SI1 Table S4), reflecting the intrinsic tendency of metal oxides to aggregate in the absence of biological stabilizers, a behavior also consistent with the rapid sedimentation and strong aggregation already described in in natural water media.[15,42]

Upon suspension in CF (Fig. 2A1–D1; SI1 Tables S1–S4), all four batches of NPs exhibited an increase in D_H, reflecting the rapid and nonspecific adsorption of proteins, *i.e.*, the soft corona. Despite their opposite bare surface charges, PS-NH_2 and PS-COOH NPs increased to 208.4 ± 3.7 and 213.7 ± 0.01 nm, respectively, suggesting similar early adsorption dynamics. Notably, AgcitLcys NPs exhibited a more pronounced size shift (from 56.8 ± 2.3 nm to 307.8 ± 8.2 nm), indicating strong interactions with CF proteins. This behavior is likely influenced by the complex surface chemistry of silver NPs functionalized with citrate and L-cysteine. TiO_2 NPs displayed the most significant increase (385.0 ± 18.6 nm), consistent with extensive early aggregation. During the subsequent 12 h, the protein corona continued to evolve and significant aggregation was observed, particularly for PS-based NPs. PS-NH_2 reached 881.5 ± 142.9 nm, PS-COOH 361.2 ± 33.23 nm, AgcitLcys 117.1 ± 2.6 nm, and TiO_2 293.9 ± 33.5 nm. After 24 h, a general reduction in D_H to similar values was observed: PS-NH_2 to 151.4 ± 2.5 nm, PS-COOH to 146.9 ± 3.5 nm, AgcitLcys to 149.5 ± 2.2 nm, whereas TiO_2 NPs remained aggregated at 237.0 ± 3.9 nm. This dimensional evolution reflected a dynamic adaptation of the

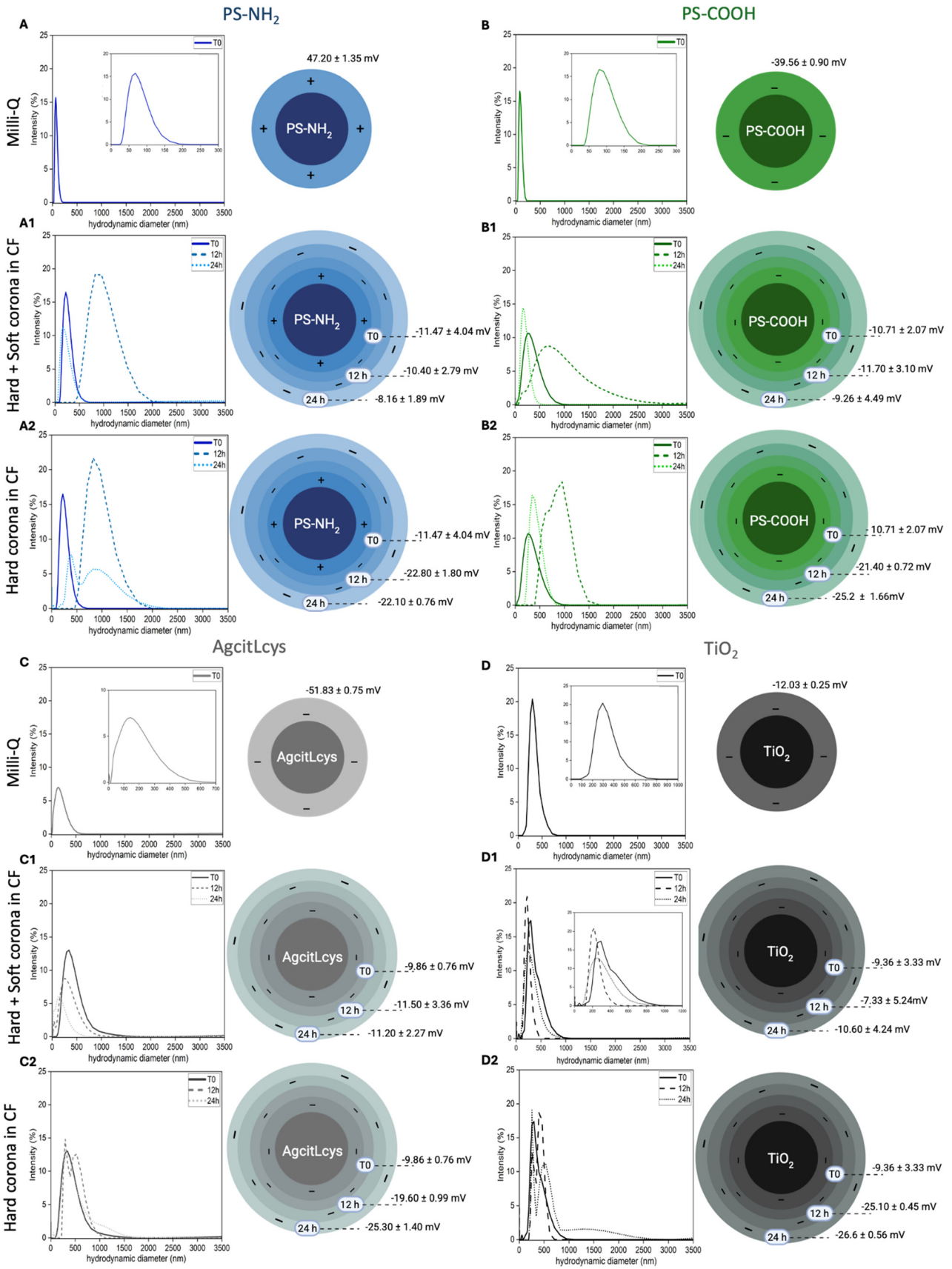

Fig. 2 Dynamic characterization of NPs by DLS and ζ_P in Milli-Q (T_0) and in CF at different time points (T_0, 12 h, 24 h). Charts A–D display the intrinsic dimensions and ζ_P of the NPs in Milli-Q. Charts A1–D1 illustrate the D_H and ζ_P evolution of the NPs in CF over time. Charts A2–D2 show the NPs following PBS washes, where only the hard corona remains.

protein corona, likely driven by the surface chemistry of the NPs and the nature of the adsorbed proteins. The initial aggregation of PS-NH_2 was significant and could be attributed to multivalent interactions between surface amine groups and CF proteins, which promoted protein bridging and aggregation.[12] Subsequent size reduction suggests reorganization of the corona into a more compact, stabilized configuration, possibly favored by the enrichment in high-affinity proteins. Similar behavior was observed for PS-COOH and AgcitLcys, suggest instead a nuanced interplay between electrostatic attraction and steric hindrance, a balance also noted by Oliani *et al.*[43] in polymeric nanocomposites, where surface ligands modulate both aggregation and colloidal stability. In the case of TiO_2, partial disaggregation may have resulted from corona restructuring mediated by the competitive adsorption of specific proteins, consistent with prior reports.[18] Although the NPs analyzed initially exhibited different surface charges, positive for PS-NH_2 and negative for PS-COOH, AgcitLcys and TiO_2, after exposure to the CF, all showed similar negative ζ_P values (−8.1 ± 1.9 to −11.2 ± 2.3 mV). This behavior reflects the dominant effect of negatively charged plasma proteins present in the CF, which preferentially adsorb onto various surfaces, effectively masking the electrostatic properties of the NPs. For PS-NH_2, in particular, a rapid shift from a positive to a negative ζ_P was observed. This charge reversal, together with the subsequent homogenization of ζ_P values between different types of NPs, are key indicators of mature corona formation and suggest that the composition of the adsorbed protein layer is the main determinant of colloidal behavior in biological environments.[17,44]

In all cases, we also characterized the hard corona by performing several washing steps on the NPs recovered from the CF after incubation as described in methods (Fig. 2A2–D2; SI1 Tables S1–S4). Already at T_0, NPs D_H increased, reflecting the selective binding of high-affinity proteins (PS-NH_2: 208.4 ± 3.7 nm; PS-COOH: 213.7 ± 5.7 nm; AgcitLcys: 307.8 ± 8.2 nm; TiO_2: 385.0 ± 44.1 nm). After 12 h, PS-NH_2, PS-COOH and TiO_2 NPs formed large aggregates, exceeding 1 μm, demonstrating that high-affinity proteins in the hard corona mediate multivalent cross-linking and promote aggregation. AgcitLcys NPs appeared slightly smaller, with an average radius of 788.2 ± 163.10 nm. This apparently counterintuitive increase of the particle size is a consequence of the removal of the soft corona, which usually provides a steric cushion preventing further NP proximity and aggregation. The compact hard corona, formed by tightly bound high-affinity proteins, fosters irreversible cross-linking and aggregation, while its rigidity limits conformational flexibility under shear, causing increased D_H, a behaviour previously observed also in Tenzer and Walkey papers,[44,45] who highlighted the critical role of the hard corona in NPs aggregation and colloidal stability. Again, size reduction was observed after 24 h (to ~602.0 ± 157.9 nm for PS-NH_2, ~530.0 ± 18.41 nm for PS-COOH, ~484.0 ± 28.9 nm for AgcitLcys, and ~1228 ± 469.3 nm for TiO_2) and in all cases the ζ_P converged to similarly negative values (from −22.1 ± 0.8 to −26.6 ± 0.6 mV).

3.2 TEM observations and dimensional variation analysis

TEM images were acquired at T_0 in Milli-Q and after 24 h in CF (Fig. 3 and SI1 Fig. S1). These observations complemented and confirmed DLS data: PS-NH_2 and PS-COOH NPs exhibited sizes closely related to their PS core in Milli-Q, with a more uniform size distribution for PS-NH_2, likely due to the increased electrostatic repulsion imparted by the surface amine groups (Fig. 3A and B). Despite their smaller nominal size and strong negative ζ_P, AgcitLcys NPs formed larger aggregates in Milli-Q. This unexpected behavior may result from the dual surface coating with citrate and L-cysteine, which could lead to uneven charge distribution or weak inter-particle interactions. Moreover, the thiol groups of L-cysteine might undergo oxidation under ambient conditions, potentially forming disulfide bridges between NPs, thus contributing to aggregate formation (Fig. 3C). TiO_2 NPs exhibited a pronounced tendency to agglomerate even in Milli-Q (Fig. 3D), consistent with previous findings reporting marked agglomeration and rapid sedimentation irrespective of ionic strength.[42,46] After 24 h in CF, a significant size increase due to protein corona formation was observed for all four batches. PS-NH_2 and PS-COOH NPs exhibited uniform, well-defined protein coatings with a thickness of 15–20 nm (Fig. 3A1 and B1), while AgcitLcys NPs showed a slightly thinner corona of 10–15 nm, indicating stable and homogeneous interactions with the proteins of the CF (Fig. 3C1). On the other hand, TiO_2 showed significant dimensional increase but a less defined corona (Fig. 3D1 and S1), likely due to lower protein affinity and stronger NP aggregation, obscuring the adsorption surface.[18,47]

Following two PBS washes, which removed weakly associated proteins, a residual hard corona of 4–9 nm persisted on both PS NPs (Fig. 3A2 and B2), while both metal-based NPs displayed a slightly thinner hard corona layer (3–5 nm, Fig. 3C2 and D2). PS-NH_2 and PS-COOH in CF suspension remained well dispersed, with only slight reductions in composite diameters, confirming the stability of the protein–NP interactions. AgcitLcys NPs also retained a visible protein layer despite aggregation in CF, whereas TiO_2 formed extensive agglomerates that were difficult to quantify accurately (Fig. S1). This observed tendency toward aggregation, particularly for TiO_2, may be attributed not only to their intrinsic colloidal instability but also to technical factors related to NP concentration during the centrifugation steps used for washing, as previously reported in the literature.[18,43]

3.3 Proteomic characterization of the hard corona

In order to assess whether the differences in the biophysical properties of the protein coronas reflected their compositional variations, we performed a biochemical and

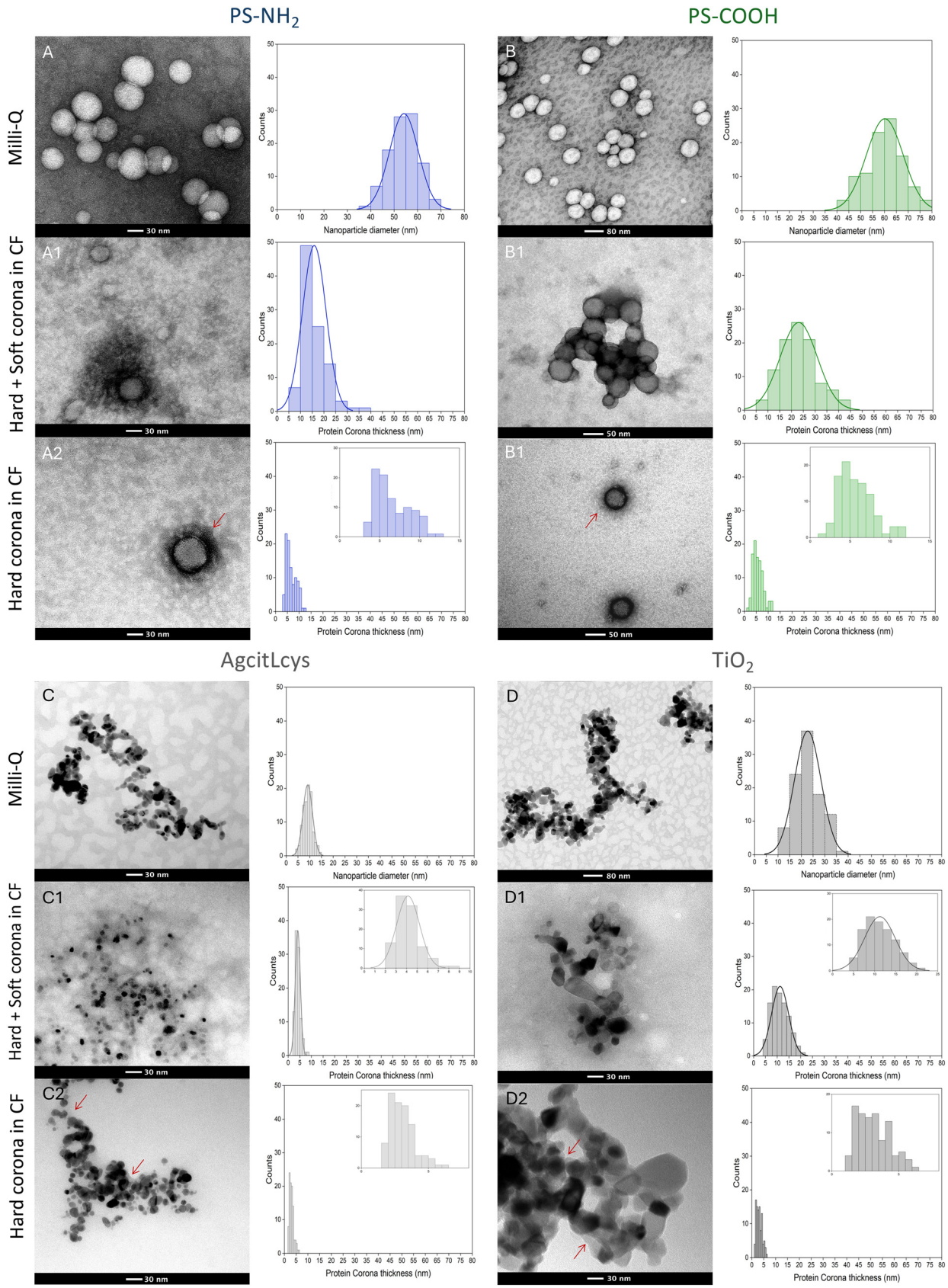

Fig. 3 Morphological and dimensional characterization of PS-NH_2, PS-COOH, AgcitLcys, and TiO_2 NPs using TEM and quantitative analysis with ImageJ. Panels A–D show the pristine morphology and size of the NPs in Milli-Q. Panels A1–D1 display the same NPs after 24 hours of incubation in CF, highlighting the formation of the protein corona (hard + soft). Panels A2–D2 show the NPs after three PBS washes, retaining only the high-affinity protein layer (hard corona); arrows indicate the residual hard corona on the NP surface.

proteomic characterization of the proteins constituting the hard corona formed on the four NPs types after 24 h of incubation in cell free CF. SDS-PAGE profiles of the detached hard corona proteins (Fig. S2) revealed well-resolved bands, ranging from <20 kDa to >250 kDa. Although a broad array of proteins was present in all samples, each NPs type exhibited a characteristic band pattern consistent with surface-chemistry-driven selectivity, as previously reported.[18,48,49] These differences among electrophoretic patterns were further validated by shotgun proteomics

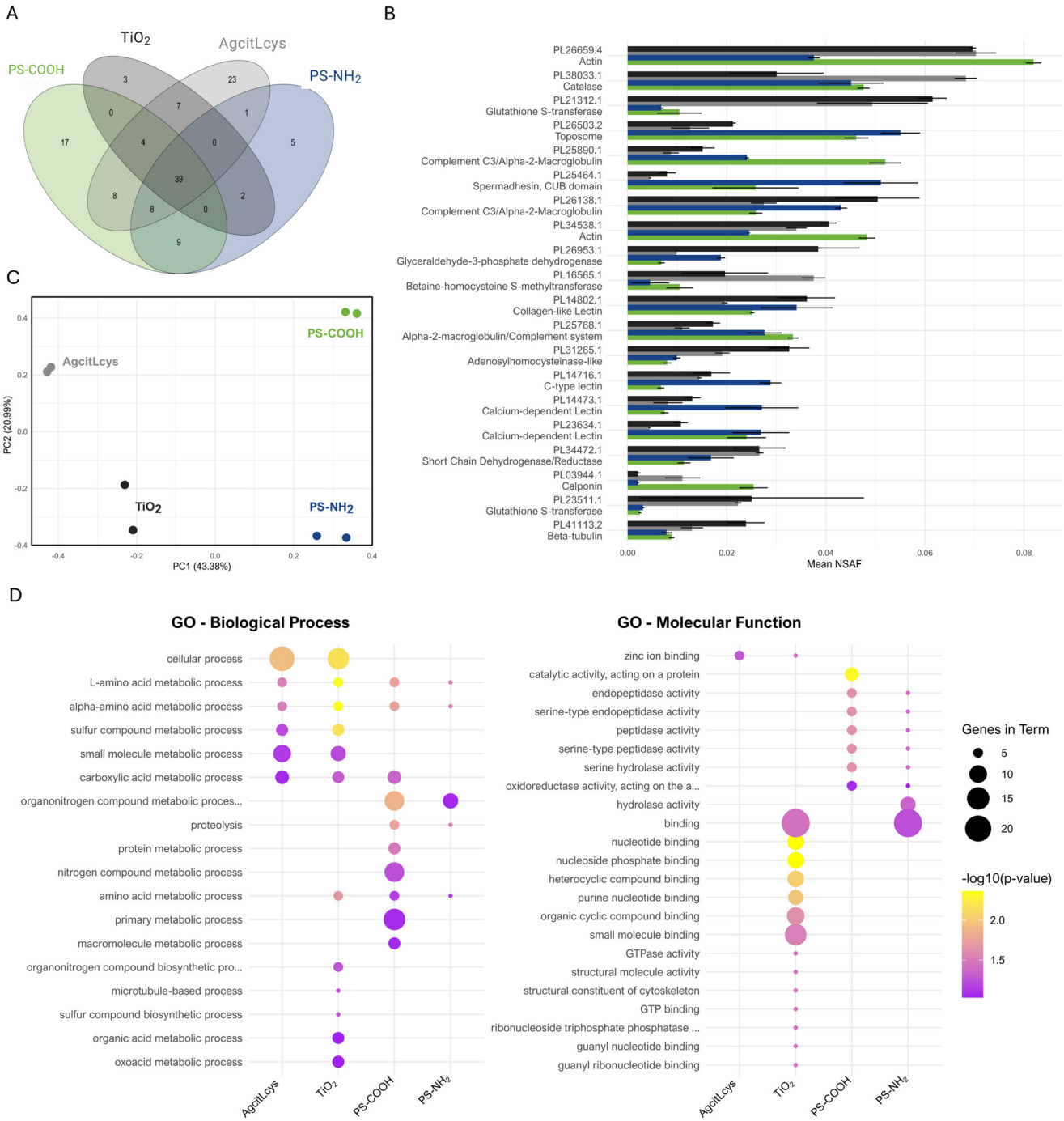

Fig. 4 Comparative proteomic characterization of the hard corona formed on four types of NPs: AgcitLcys, PS-NH_2, PS-COOH and TiO_2, after incubation in cell-free CF of *P. lividus*. A) Venn diagram showing the number of unique and shared proteins among the four NP types. B) Bar plot representing the relative abundance (NSAF) of the 20 most significant proteins across all coronas. C) PCA summarizing the similarity and clustering of protein profiles associated with each NP type. D) GO enrichment analysis showing the top biological processes and molecular functions represented in the protein coronas of each NP. In panel D, circle size reflects the number of proteins associated with each GO term, while color intensity represents the statistical significance of enrichment (logarithm of the adjusted *p*-value).

analyses: a total of 126 proteins were identified across all experimental conditions (Fig. 4A and S2), of which only 39 (31%) were shared by the four NP batches.

On the other hand, several unique proteins were found for each of the four NPs, and specifically 23 for AgcitLcys, 17 for PS-COOH, 5 for PS-NH_2 and only 3 for TiO_2 (Fig. 4A and S2). This highlights possible selectivity of each type of NPs in capturing proteins based on their surface chemistry and behaviour in the water media. To better compare the protein content of the coronas assembled on the different NPs, we performed a label free quantification of the absorbed proteins by calculating, for each condition, the normalized spectral abundance factors (NSAF), which provide an estimate of the relative abundance of each protein within the sample. Fig. 3B shows the distribution of the 20 most abundant proteins detected in the four NPs and their relative abundance on each NP. Interestingly, while the overall distribution was globally conserved, a few cases emerged of proteins that seemed to be preferentially absorbed on PS NPs, independently on their surface functionalization. This is the case, for instance, of the complement C3 proteins (PL25890.1 and PL25768.1), of spermadhesin (PL25464.1) and of the toposome (Major Yolk Protein, MYP), which is the most abundant protein within the CF. On the other hand, proteins belonging to specific enzyme superfamilies, such as the glutathione-*S*-transferases (PL21312.1 and PL23511.1), the betaine-homocysteine-*S*-methyl transferase (PL16565.1) and other more generally involved in the redox balance were relatively more abundant in the corona of metal-based NPs. This observation suggests that the composition of the hard corona does not directly reflect the relative protein abundances in the CF.

Globally, our analysis highlighted the existence of a closest relationship between the coronas formed on PS NPs, regardless functionalization, *vs.* metal-based NPs, as better summarized by the results of the PCA performed on the proteins' calculated NSAFs (Fig. 4C). This is consistent with previous findings,[50] showing that silica and PS NPs acquire markedly different coronas when incubated in the same medium, due to their distinct surface chemistries. These results are also in agreement with quantitative proteomic analyses of metallic NPs, reporting between 33 and 37% overlap in corona proteins between AuNPs and AgNPs after incubation in human serum.[51,52] Similarly, previous studies by 2D electrophoresis followed by MS analyses highlighted only marginal variations in the hard corona of PS-NH_2 *vs.* PS-COOH NPs, consistent with their identical PS cores and incubation protocols. This indicates that, in the absence of differences in the NP core-composition, surface functionalization primarily modulates the relative abundances of secondary corona constituents, rather than reshaping the dominant protein portion.[12]

On the other hand, several unique proteins have been detected in each condition, particularly for AgcitLcys and PS-COOH NPs, (Table 1). Among the 23 proteins uniquely identified in the hard corona of AgcitLcys NPs, approximately one-third belong to well-known antioxidant families. These include three glutathione *S*-transferases (PL22978.1, PL22170.1, PL23506.1), an aldo-keto reductase (PL23316.1), and a partial glutaredoxin (PL23511.1), all enzymes involved in neutralizing reactive oxygen species

Table 1 Unique proteins detected in the hard corona of AgcitLcys and PS-COOH NPs after 24 h of incubation in *P. lividus* CF. The table lists protein IDs and corresponding InterPro annotation

AgcitLcys		PS-COOH	
Protein ID	InterPro annotation	Protein ID	InterPro annotation
PL30406.1	Adenylate kinase/UMP-CMP	PL07830.1	Cueball/EGF/LRP/nidogen
PL08543.1	Inositol monophosphatase-like	PL07343.1	—
PL16055.1	Short-chain dehydrogenase/reductase	PL36227.2	Fibrocystin
PL22978.1	Glutathione *S*-transferase superfamily	PL03114.1	Scavenger receptor cysteine-rich
PL25915.3	Kynurenine–oxoglutarate transaminase	PL00623.1	—
PL22170.1	Glutathione *S*-transferase	PL09805.5	Lipocalin
PL38374.1	Transaldolase/fructose-6-phosphate aldolase	PL29004.1	Alpha-2-macroglobulin/complement system
PL20764.1	Regucalcin (Ca)	PL05728.2	Complement and asymmetry regulator
PL10208.1	Zinc-containing quinone oxidoreductase	PL02224.1	Vitellogenin/apolipophorin
PL23511.1	Glutaredoxin (partial)	PL34921.1	Protein disulphide isomerase
PL30422.1	14-3-3 protein	PL39025.1	Endoglin/TGF-beta receptor type III
PL27336.1	P-loop containing nucleotide triphosphate hydrolase	PL26698.1	Peptidase S1A, chymotrypsin family
PL31241.1	Peroxisomal sarcosine oxidase	PL13592.1	Malate dehydrogenase, type 1
PL22951.1	P-loop containing nucleoside triphosphate hydrolase	PL25700.1	Scavenger receptor cysteine-rich
PL22992.1	Inorganic pyrophosphatase (Mg)	PL04694.1	Calcium-dependent lectin
PL26998.2	P-loop containing nucleoside triphosphate hydrolase	PL17524.1	Ezrin/radixin/moesin-like
PL01820.1	Sorbitol dehydrogenase-like	PL00368.1	Tropomyosin
PL32335.2	Short-chain dehydrogenase/reductase SDR		
PL28243.1	P-loop containing nucleoside triphosphate hydrolase		
PL23316.1	Aldo-keto reductase		
PL23506.1	Glutathione *S*-transferase		
PL31299.1	Peroxisomal sarcosine oxidase		
PL38692.1	Ankyrin repeat-containing domain superfamily		

(ROS) and detoxifying oxidized biomolecules. Also present is a zinc-containing quinone oxidoreductase (PL10208.1), which may prevent semiquinone radical formation, along with several short-chain dehydrogenases/reductases (PL16055.1, PL32335.2, PL01820.1), a large family of NAD-dependent oxidoreductases with broad substrate specificity. The corona also includes key metabolic regulators, such as adenylate kinase (PL30406.1), which balances cellular levels of ATP, ADP, and AMP, and transaldolase (PL38374.1), an enzyme in the pentose phosphate pathway that supports NADPH production. These are accompanied by four P-loop NTP hydrolases (PL27336.1, PL22951.1, PL26998.2, PL28243.1) and an inorganic pyrophosphatase (PL22992.1), proteins involved in nucleotide turnover and phosphate homeostasis. In addition, proteins associated with intracellular signaling were identified, including a 14-3-3 protein (PL30422.1), a scaffold that regulates kinases and phosphoproteins, and regucalcin (PL20764.1), which modulates calcium homeostasis and metabolic regulation. Two peroxisomal sarcosine oxidases (PL31241.1, PL31299.1), possibly involved in hydrogen peroxide (H_2O_2) production and amino acid catabolism, and an ankyrin-repeat protein (PL38692.1) of unknown function completed the profile.

The unique PS-COOH corona protein profile revealed instead a strong extracellular and immunogenic protein content, in contrast to the metabolically active, redox-focused corona observed for AgcitLcys NPs. Among the most represented protein families, we detected several components involved in innate immune responses, including two scavenger receptor cysteine-rich (SRCR) domain proteins (PL03114.1, PL25700.1), an alpha-2-macroglobulin/complement-like factor (PL29004.1), and a complement/asymmetry regulator (PL05728.2). The corona also included proteins involved in transport and signaling, such as vitellogenin/apolipophorin (PL02224.1), a key lipoprotein in reproduction and lipid transfer, and a lipocalin (PL09805.5), a lipid transporter. Several proteins with structural or cytoskeletal functions were identified, including ezrin/radixin/moesin-like protein (PL17524.1), tropomyosin (PL00368.1), fibrocystin (PL36227.2), and a chymotrypsin-like serine peptidase (PL26698.1), as well as Cueball/EGF/LRP/nidogen-domain protein (PL07830.1), endoglin/TGF-beta receptor type III (PL39025.1), and protein disulfide isomerase (PL34921.1), which are also involved in cellular architecture, cytoskeletal organization, and membrane-associated scaffolding, all of which reinforce the extracellular and surface-oriented profile of this corona.

From Table 1 (see SI2), the divergent corona compositions of AgcitLcys and PS-COOH NPs directly reflect their distinct surface chemistries and thereby define their biological identities. AgcitLcys NPs, comprising an Ag^0/Ag^+ core enveloped by a citrate/L-cysteine bilayer, present both deprotonated carboxylate ($–COO^-$) and thiolate ($–S^-$) moieties. The thiolate groups facilitate strong coordination with cysteine residues and histidine imidazole nitrogens on protein surfaces, while the carboxylates attract lysine- and arginine-rich domains *via* long-range electrostatic interactions. The combination of carboxylate and thiolate groups therefore represents a plausible physicochemical basis for selective protein adsorption on AgcitLcys NPs. Because coronas were generated in cell-free CF, the resulting protein composition reflects affinity-driven interactions with the pre-existing CF proteome rather than active biological responses to NP exposure. Within this context, the marked enrichment of intracellular enzymes, particularly those involved in redox catalysis and energy metabolism, suggests a preferential association with redox-sensitive proteins that could contribute to perturbation of oxidative homeostasis and to potential pro-oxidant activity.

Conversely, PS-COOH NPs lack redox-active metal centers and instead display a uniformly hydrophilic, negatively charged carboxylate surface. Their corona is thus formed predominantly through electrostatic attraction and hydrogen bonding with extracellular matrix and immune-related proteins, including lectins, complement factors, and adhesion molecules. Such interactions yield a comparatively inert protein coating that is likely to favor recognition and clearance by phagocytic systems, without directly compromising key intracellular enzymatic pathways. Consequently, PS-COOH exhibits a more benign biological profile than AgcitLcys, underscoring the critical importance of surface chemistry in dictating NP–protein corona formation, subsequent biodistribution, and ecotoxicological outcome.

In order to correlate the proteomic profiles with potential biological and ecotoxicological outcomes, we performed a GO enrichment analysis on the proteins detected on each batch of NPs, using as background the total proteome characterized (Fig. 4D). Although suffering from limitations from the low number of proteins in the samples, the analysis provided a qualitative overlook of the enrichment of terms related to specific biological processes and molecular functions. Specifically, as anticipated, the protein corona of AgcitLcys NPs was enriched in oxidoreductases, but also hydrolases, serine-type peptidases, and proteins binding metals and nucleotides. This composition reflects the bifunctional citrate–L-cysteine surface coating and the thiol-rich nature of the marine CF.[45,53] Such a profile predicts strong ROS generation, extracellular matrix degradation, and selective Ag^+ release in acidic intracellular compartments such as lysosomes mechanisms, that correlates with the immunotoxic effects observed in *P. lividus* coelomocytes in this study (see *in vitro* results). Although the citrate/L-cysteine coating confers greater colloidal stability compared to commonly used commercial silver NP (AgNP) formulations, only partial complexation of Ag^+ occurs in high ionic strength water solutions (*e.g.*, seawater), where chloride ions (Cl^-) can bind to AgcitLcys, limiting its availability. Nevertheless, a fraction of Ag^+ remains bioavailable and may contribute to biological effects. This residual ionic release, potentially enhanced under acidic conditions such as those found in

lysosomes, could help explain the selective recruitment of redox-active and detoxifying proteins within the corona.[41,54]

Similarly, the TiO_2 NP corona was enriched in GTPases, purine-binding proteins, and microtubule components, a pattern that is consistent with activation of endocytic pathways and cytoskeletal remodeling, potentially facilitating uptake. The functional profile was more oriented toward redox and metabolic regulation than the "adhesive" coronas previously described by Alijagic *et al.*[18] dominated by lectins and adhesion proteins. It is important to note that Alijagic's study relied primarily on immunoblotting for protein identification rather than LC-MS/MS-based analysis used in the present study. While immunoblotting-based analyses are inherently targeted toward a limited number of predefined proteins, our approach provides a broader and more unbiased characterization of hard corona composition, enabling the detection of less abundant proteins and expanding previous results. As later shown by the same group,[47] the TiO_2 corona can induce a transient immunometabolic tolerance by downregulating NF-κB and MAPK14 and activating antioxidant pathways, potentially leading to progressive redox imbalance and oxidative stress.

As for the polymeric NPs, previous findings revealed that PS-COOH and PS-NH_2 shared a core of metabolic enzymes involved in carbohydrate, oxoacid, and organic compound turnover, but displayed marked functional specialization.[12] PS-COOH was mainly enriched in hydrolases, peptidases, and peptidase inhibitors, consistent with the affinity of negatively charged surfaces for enzyme regulators that protect against excessive proteolysis.[55] In contrast, PS-NH_2 NPs coronas were enriched in enzymes involved in sulfur, organonitrogen, and nucleotide metabolism, as well as in nucleotide-binding proteins and cytoskeletal components. These features are consistent with enhanced activation of redox pathways and endocytic mechanisms such as macropinocytosis, in agreement with previous findings in *P. lividus* and *M. galloprovincialis*.[14,56]

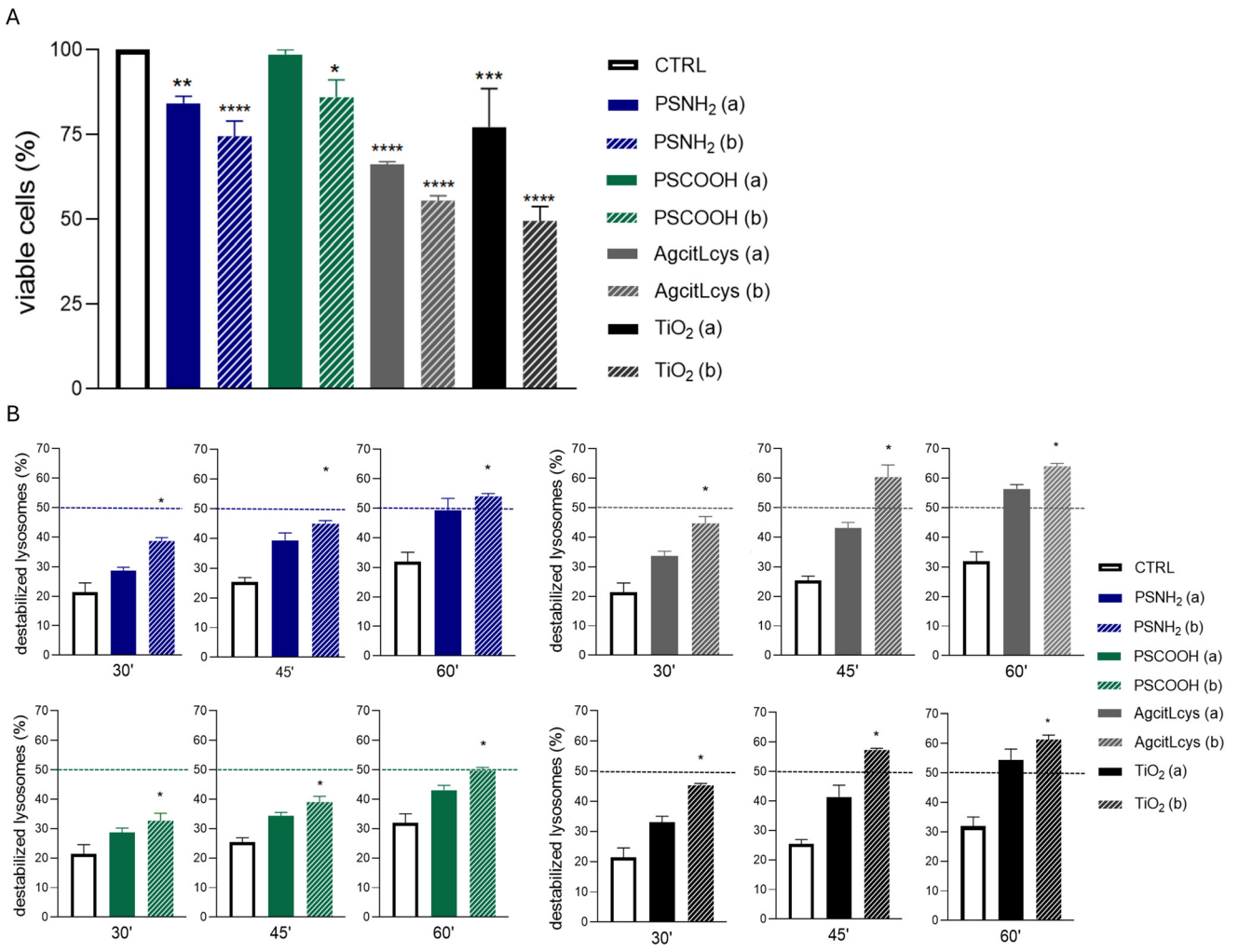

Fig. 5 A) Percentage of viable coelomocytes relative to the total number of cells analyzed following exposure to each NP type at (a) 25 μg L^{-1} and (b) 25 μg mL^{-1}. B) Lysosomal membrane stability expressed as the percentage of coelomocytes showing destabilized lysosomes, assessed by the NRRT assay (100 cells scored per replicate). Significance levels are indicated as *$p < 0.05$, **$p < 0.01$, ***$p < 0.001$, ****$p < 0.0001$.

The characterization of NP size, surface charge, and protein corona composition provides a crucial foundation for understanding their biological behavior and overall impacts. Our results demonstrate that the composition of the hard protein corona is strongly dictated by the surface chemistry of the NPs, shaping not only the nature of adsorbed proteins but also their functional identity and relative abundance. Metal-based NPs, AgcitLcys and TiO_2, formed coronas enriched in redox-active enzymes and intracellular regulators, indicating a higher potential for cellular interaction and biological reactivity. These observations suggest a more pronounced biological reactivity, which may translate into cytotoxic effects in marine invertebrate immune cells.

In contrast, PS-based NPs formed coronas dominated by metabolic and extracellular proteins, with PS-COOH showing a profile suggestive of regulatory and protective interactions, and PS-NH_2 reflecting a more active engagement in redox and uptake-related processes. These distinct profiles suggest a more moderate and surface-functionalization-dependent biological impact compared to metal-based NPs. Taken together, these findings provide a mechanistic framework to interpret the results of subsequent ecotoxicological investigations on *P. lividus* coelomocytes.

3.4 Ecotoxicological assays on *P. lividus* coelomocytes

Following the characterization of NPs incubated in the CF of *P. lividus*, we proceeded to assess the associated ecotoxicological effects. The selected biological endpoints were coelomocyte viability, lysosomal membrane stability, and the relative abundance of red cells (Fig. 5), used as functional indicators of coelomocytes health status.[25] The effects of different types of NPs on coelomocytes were investigated at two concentrations: one environmentally relevant (25 μg L^{-1}) and one representing an acute exposure scenario (25 μg mL^{-1}).[57–59] The results clearly showed that both the surface chemistry of the NPs and the functional composition of the associated protein corona are key determinants of sea urchin immune cell responses.

The analysis of coelomocyte viability revealed distinct effects depending on NP type and concentration. PS-COOH NPs had no significant effect on cell viability at either concentration tested, whereas PS-NH_2 NPs led to a moderate, yet statistically significant, reduction in viability, particularly at a concentration of 25 μg mL^{-1} (Fig. 5A). This suggests that amino-modified PS NPs exhibit more intense cellular interaction and may induce intracellular stress. Both metal-based NPs, AgcitLcys and TiO_2, caused concentration-dependent decreases in cell viability, with effects observable even at lower concentrations (Fig. 5A). AgcitLcys NPs triggered the strongest reduction (~50% at 25 μg mL^{-1}), while TiO_2 induced a milder reduction. The observed results indicate that assessing coelomocytes viability is a sensitive and early indicator of sub-lethal cytotoxicity. This is particularly useful for monitoring the effects of NPs-induced stress under ecologically relevant conditions. This biomarker integrates information about particle–cell interaction, intracellular accumulation, and potential alterations in metabolic and homeostatic processes.

Lysosomal membrane stability was also investigated as a complementary endpoint, to further explore NP-induced stress and internalization dynamics. Lysosomes are key organelles in immune cells such as coelomocytes, responsible for degrading internalised materials and regulating intracellular homeostasis. Their structural integrity is therefore particularly sensitive to xenobiotic exposure and oxidative imbalance. Disruption of lysosomal membranes is a well-established marker of sublethal stress, providing early insight into the cytotoxic mechanisms induced by NPs. Using the neutral red retention time (NRRT) assay, we observed that all four types of NPs caused an increase in lysosomal destabilisation that was dependent on concentration. The most pronounced effects were again induced by AgcitLcys and TiO_2 NPs, leading to nearly 50% of cells exhibiting destabilised lysosomes at the highest tested concentration (25 μg mL^{-1}, Fig. 5B). PS-NH_2 induced moderate yet statistically significant destabilisation, while PS-COOH had only a minimal impact, confirming its relative biocompatibility (Fig. 5B). These results align with previous findings in *P. lividus* and other marine invertebrates, where metal-based NPs have been shown to compromise lysosomal integrity.[17,60,61] The limited impact of PS-COOH NPs can be explained in light of studies from both marine and mammalian systems, which have demonstrated that the surface charge of NPs plays a critical role in modulating their intracellular fate and associated toxicity.[62,63] Negatively charged NPs, such as PS-COOH, tend to escape from the lysosomal compartment and interact with other subcellular targets, potentially triggering mild cellular stress without directly disrupting lysosomal membranes.[14,64,65] Conversely, positively charged NPs like PS-NH_2 are more likely to destabilise lysosomes *via* the proton sponge effect, causing osmotic swelling, membrane rupture, and the generation of reactive oxygen species (ROS), which in turn activate broader damage pathways.[66] These mechanisms are reflected in the observed lysosomal responses, reinforcing the relevance of lysosomal membrane stability as a sensitive and mechanistically informative assay of sublethal cellular dysfunction under environmentally realistic exposure scenarios.

Finally, we assessed the relative abundance of coelomocytes, which offers an additional, functionally relevant biomarker for evaluating immune activation in *P. lividus*. In this species, in fact, pigmented cells known as red spherule cells play a central role in innate immunity due to their content of echinochrome A, a pigment with well-documented antioxidant, antimicrobial, and iron-chelating properties.[26,67] Upon immune challenge or cellular stress, the number of red spherule cells can increase, likely through mobilization from internal reservoirs or local proliferation. This cellular response contributes to the organism's defence against pathogens and environmental stressors, highlighting the importance of these cells as sensitive

indicators of immune activation.[25,67,68] In our experiments, exposure to all types of NPs resulted in an increase in the frequency of red cells compared to controls, although with high variability between individuals and experimental replicates, as shown in Fig. S3/Table S6. This variability was independent of core composition, particle size or NP concentration; rather, it reflects the well-documented plasticity of the invertebrate immune system.[67,69] Despite the high variability, the overall direction of the response consistently pointed toward an increase in red cells, suggesting that NPs are recognized as foreign stimuli and trigger a protective or inflammatory response. This behavior is consistent with previous studies on the sea urchin *P. lividus* to the pesticide lindane, which showed an increased proportion of red cells even as total coelomocyte counts decreased.[70] Similarly, a significant rise in pigmented and non-pigmented spherule cells was reported in tropical sea urchins subjected to thermal stress, supporting their role as sensitive stress biomarkers.[69] However, the red cell response appears to be a rather non-specific or generalized indicator of immune activation, especially compared to more targeted biomarkers, such as cell viability or lysosomal stability. In this context, the lack of statistically significant changes in red cell proportions across treatments may be attributed to the broad, non-selective nature of this response, which may not discriminate sharply between different types or concentrations of NPs. Furthermore, the relatively short exposure time of 4 h may have been insufficient to elicit robust or distinguishable red cell responses across experimental groups. This time window reflects a technical limitation widely recognized in echinoderm cell culture systems, as coelomocytes rapidly lose viability and functional integrity beyond 4–5 hours post-extraction, even under carefully controlled conditions.[37,41,54,71,72] The inability to maintain coelomocytes *in vitro* for extended periods represents a key constraint in the design of longer-term ecotoxicological assays and may hinder the detection of more delayed or cumulative immune responses.

Overall, the ecotoxicological responses observed in *P. lividus* coelomocytes reflected distinct mechanisms of action associated with each NP type. The pronounced cytotoxic and lysosomal effects induced by AgcitLcys were likely the result of multiple, interconnected processes. In addition to NP-specific properties and the biological identity conferred by the protein corona, a key contributing factor is the partial release of bioavailable Ag^+ ions from the NP surface. Silver NPs are well known to undergo surface oxidation and dissolution in aqueous media, particularly under high ionic strength conditions such as seawater. The citrate/L-cysteine coating used for AgcitLcys provides improved colloidal stability but does not fully prevent ion exchange processes. As demonstrated by Bellingeri *et al.*,[72] the nature of the capping layer critically determines dissolution kinetics and the resulting (eco)toxicity of AgNPs, with residual silver release remaining an important driver of biological effects even for coated formulations. In biological fluids, adsorbed proteins forming the corona can further modulate surface reactivity and silver speciation, potentially influencing cellular delivery. Previous investigations on aquatic invertebrate cells indicate that internalized AgNPs are typically trafficked to acidic intracellular compartments such as endosomes and lysosomes.[40,53,72] Under these conditions, protonation and ligand exchange reactions may enhance Ag^+ liberation from the particle surface. Free or weakly complexed Ag^+ ions are known to be highly reactive toward cellular thiol groups and can bind to cysteine-rich proteins, potentially disrupting enzymatic activity and weakening antioxidant defenses. Although these processes were not directly measured in the present study, they provide a plausible mechanistic framework to interpret the strong biological effects observed for AgcitLcys NPs. In this context, the enrichment of redox-related and detoxification enzymes detected in the AgcitLcys corona is consistent with the propensity of AgNPs to interact with proteins involved in oxidative stress regulation. In contrast, TiO_2 NPs, while still eliciting measurable biological responses, exerted milder effects, consistent with their recognized biopersistence and lower reactivity in marine invertebrate models. The milder cellular response elicited by TiO_2 NPs aligns with previous results by Alijagic *et al.*,[18] on the formation of a protein corona around TiO_2 particles incubated in CF. This corona facilitates an organised pattern of cellular uptake without causing morphological or functional alterations. Subsequent studies have described transient downregulation of inflammatory genes and upregulation of antioxidant pathways in TiO_2 exposed coelomocytes, suggesting a temporary state of immunometabolic tolerance.[47] Furthermore, TiO_2 has been shown to stimulate phagocytic activity *via* TLR/p38 MAPK signalling, which supports the hypothesis that the protein corona orchestrates a biologically recognised and physiologically regulated interaction.[18] The moderate toxicity associated with PS-NH_2 NPs may be ascribed not only to their originally positive surface charge, which facilitates protein adsorption and initial cellular uptake, but also to the composition of their acquired protein corona. Upon incubation in CF, PS-NH_2 particles tend to develop a corona enriched in stress-related and immunomodulatory proteins, which, despite reversing the net surface charge to negative, can still promote internalization and destabilization of lysosomal membranes. In contrast, the negligible impact of PS-COOH NPs supports the notion that their corona composition leads to reduced cellular interaction and minimal subcellular disruption. These findings align with previous studies in sea urchin coelomocytes, supporting a particle-type-specific pattern of biological interaction and ecotoxicity. Several studies have confirmed that cationic NPs disrupt homeostasis through increased internalization and stimulation of oxidative pathways, ultimately leading to cytotoxicity.[12,14,17,50] These results acquire stronger significance in light of the above proteomic characterization of the hard corona formed around the NPs. The protein composition clearly reflected

the physicochemical nature of the particles and exhibited a strong correlation with the observed biological effects.

PS-COOH and PS-NH_2 NPs exhibited divergent protein corona profiles. The corona of PS-COOH was enriched in proteins involved in extracellular immune recognition and modulation of inflammatory responses. Protease inhibitors may help reduce inflammation by protecting tissues from proteolytic stress, while lectins and complement proteins promote controlled, non-inflammatory immune recognition. This proteomic pattern is consistent with the observed higher biocompatibility, suggesting low levels of cellular internalization and immune activation. In contrast, PS-NH_2 coronas contain redox enzymes, cytoskeletal proteins, and metabolic enzymes involved in sulfur and nitrogen cycling. The presence of redox enzymes indicates the occurrence or anticipation of oxidative stress, whereas cytoskeletal proteins may reflect or promote active internalization and cellular reorganization. These features suggest that PS-NH_2 are rapidly internalized by coelomocytes, triggering subcellular stress and functional alterations, consistent with the observed effects on cell viability and lysosomal destabilization.

Metal-based NPs, AgcitLcys and TiO_2, displayed partially overlapping proteomic signatures, including oxidoreductases, glutathione *S*-transferases, and metal-binding proteins, all involved in detoxification and redox regulation. Notably, the coronas of AgcitLcys NPs were particularly enriched in stress-related proteins and immune mediators, suggesting a high affinity for molecules typically associated with oxidative and inflammatory responses. This composition may predispose the NPs to trigger such pathways upon cellular interaction, potentially exacerbated by the release of Ag^+ ions, known to disrupt cellular structures and inhibit antioxidant defenses. Conversely, the coronas of TiO_2 were characterized by a higher representation of GTPases and cytoskeletal remodeling proteins, supporting a controlled internalization mechanism and adaptive cellular responses, in line with the milder effects observed on coelomocytes.

The observed toxicity gradient (AgcitLcys > TiO_2 > PS-NH_2 > PS-COOH) mirrored the functional roles of the corona-associated proteins, highlighting how specific protein sets can modulate particle–cell interactions, internalization capacity, and the activation of pro-inflammatory or adaptive cellular responses. In this context, the protein corona composition emerges as a mechanistic link between NP identity and biological impact, reinforcing the relevance of *P. lividus* coelomocytes as a sensitive and informative model for marine nanotoxicology.

Conclusions

This study provides an integrated view of how engineered NPs interact with the CF of *P. lividus*, highlighting the role of the protein corona in modulating biological outcomes at the cellular level. By combining physical characterization (DLS and TEM), proteomic profiling, and ecotoxicological bioassays, we demonstrate that both the core composition and surface functionality of NPs dictate distinct patterns of protein adsorption and, in turn, influence cellular responses such as viability, lysosomal stability, and immune activation. Our findings reinforce the pivotal role of the protein corona as a molecular interface that governs NP–cell interactions, determining recognition, internalization, and downstream biological effects. In this context, corona composition analysis emerged as a crucial step for understanding NPs behavior in biological fluids and should be considered a key element in nanosafety assessment strategies. Additionally, the selected functional endpoints-cell viability, lysosomal membrane stability, and red cell activation, proved to be sensitive and informative endpoints and biomarkers for detecting sublethal stress in marine invertebrates under environmentally relevant conditions. These results confirm the suitability of sea urchin coelomocytes as a robust and ecologically relevant model for marine nanotoxicology. Taken together, this work contributes to the development of safer nanomaterials by identifying compositional and functional traits that correlate with reduced ecotoxicity. The integration of proteomic and cellular-level functional analyses offers valuable insights for regulatory frameworks and future safe-by-design approaches aimed at minimizing the environmental and biological risks associated with NP exposure.

Conflicts of interest

The authors declare that they have no known competing financial interests or personal relationships that could have appeared to influence that work reported in this paper.

Data availability

All data generated and analysed during this study are included in this published article and its supplementary information (SI). No additional datasets were generated or analysed.

Supplementary information is available. See DOI: https://doi.org/10.1039/d5en00836k.

References

1 M. P. Monopoli, C. Åberg, A. Salvati and K. A. Dawson, Biomolecular coronas provide the biological identity of nanosized materials, *Nat. Nanotechnol.*, 2012, **7**(12), 779–786, DOI: 10.1038/nnano.2012.207.

2 M. Hadjidemetriou and K. Kostarelos, Evolution of the nanoparticle corona, *Nat. Nanotechnol.*, 2017, **12**(4), 288–290, DOI: 10.1038/nnano.2017.61.

3 G. V. Lowry, Opportunities and challenges for nanotechnology in the agri-tech revolution, *Nat. Nanotechnol.*, 2019, **14**(6), 517–522, DOI: 10.1038/s41565-019-0461-7.

4 A. A. Keller, S. McFerran, A. Lazareva and S. Suh, Global life cycle releases of engineered nanomaterials, *J. Nanopart. Res.*, 2013, **15**(6), 1692, DOI: 10.1007/s11051-013-1692-4.

5 J. R. Lead, G. E. Batley and P. J. J. Alvarez, *et al.*, Nanomaterials in the environment: Behavior, fate,

bioavailability, and effects—An updated review, *Environ. Toxicol. Chem.*, 2018, **37**(8), 2029–2063, DOI: 10.1002/etc.4147.

6 A. A. González-Fernández, M. Aceves-Mijares, O. Pérez-Díaz, J. Hernández-Betanzos and C. Domínguez, Embedded Silicon Nanoparticles as Enabler of a Novel CMOS-Compatible Fully Integrated Silicon Photonic Platform, *Crystals*, 2021, **11**(6), 630, DOI: 10.3390/cryst11060630.

7 E. Besseling, J. T. K. Quik, M. Sun and A. A. Koelmans, Fate of nano- and microplastic in freshwater systems: A modeling study, *Environ. Pollut.*, 2017, **220**, 540–548, DOI: 10.1016/j.envpol.2016.10.001.

8 C. J. Dedman, Nano-ecotoxicology in a changing ocean, *SN Appl. Sci.*, 2022, **4**(10), 264, DOI: 10.1007/s42452-022-05147-0.

9 A. Brunelli, V. Cazzagon and E. Faraggiana, *et al.*, An overview on dispersion procedures and testing methods for the ecotoxicity testing of nanomaterials in the marine environment, *Sci. Total Environ.*, 2024, **921**, 171132, DOI: 10.1016/j.scitotenv.2024.171132.

10 S. Feng, L. Zhu and X. Zhao, *et al.*, Ecological risk assessment of metallic nanoparticles on the marine environments: Species sensitivity distributions analysis, *Front. Mar. Sci.*, 2022, **9**, 985195, DOI: 10.3389/fmars.2022.985195.

11 L. Canesi, T. Balbi and R. Fabbri, *et al.*, Biomolecular coronas in invertebrate species: Implications in the environmental impact of nanoparticles, *NanoImpact*, 2017, **8**, 89–98, DOI: 10.1016/j.impact.2017.08.001.

12 G. Grassi, C. Landi, C. D. Torre, E. Bergami, L. Bini and I. Corsi, Proteomic profile of the hard corona of charged polystyrene nanoparticles exposed to sea urchin Paracentrotus lividus coelomic fluid highlights potential drivers of toxicity, *Environ. Sci.: Nano*, 2019, **6**, 2937–2947, DOI: 10.1039/c9en00824a.

13 K. Pikula, A. Zakharenko and V. Chaika, *et al.*, Toxicity of Carbon, Silicon, and Metal-Based Nanoparticles to Sea Urchin Strongylocentrotus intermedius, *Nanomaterials*, 2020, **10**(9), 1825, DOI: 10.3390/nano10091825.

14 L. F. Marques-Santos, G. Grassi and E. Bergami, *et al.*, Cationic polystyrene nanoparticle and the sea urchin immune system: biocorona formation, cell toxicity, and multixenobiotic resistance phenotype, *Nanotoxicology*, 2018, **12**(8), 847–867, DOI: 10.1080/17435390.2018.1482378.

15 C. Della Torre, E. Bergami and A. Salvati, *et al.*, Accumulation and Embryotoxicity of Polystyrene Nanoparticles at Early Stage of Development of Sea Urchin Embryos Paracentrotus lividus, *Environ. Sci. Technol.*, 2014, **48**(20), 12302–12311, DOI: 10.1021/es502569w.

16 C. Murano, E. Bergami, G. Liberatori, A. Palumbo and I. Corsi, Interplay Between Nanoplastics and the Immune System of the Mediterranean Sea Urchin Paracentrotus lividus, *Front. Mar. Sci.*, 2021, **8**, 647394, DOI: 10.3389/fmars.2021.64739.

17 V. Matranga and I. Corsi, Toxic effects of engineered nanoparticles in the marine environment: model organisms and molecular approaches, *Mar. Environ. Res.*, 2012, 32–40, DOI: 10.1016/j.marenvres.2012.01.006.

18 A. Alijagic, O. Benada, O. Kofroňová, D. Cigna and A. Pinsino, Sea Urchin Extracellular Proteins Design a Complex Protein Corona on Titanium Dioxide Nanoparticle Surface Influencing Immune Cell Behavior, *Front. Immunol.*, 2019, **10**, 2261, DOI: 10.3389/fimmu.2019.02261.

19 A. Pinsino, R. Russo, R. Bonaventura, A. Brunelli, A. Marcomini and V. Matranga, Titanium dioxide nanoparticles stimulate sea urchin immune cell phagocytic activity involving TLR/p38 MAPK-mediated signalling pathway, *Sci. Rep.*, 2015, **5**(1), 14492, DOI: 10.1038/srep14492.

20 A. Alijagic, F. Barbero and D. Gaglio, *et al.*, Gold nanoparticles coated with polyvinylpyrrolidone and sea urchin extracellular molecules induce transient immune activation, *J. Hazard. Mater.*, 2021, **402**, 123793, DOI: 10.1016/j.jhazmat.2020.123793.

21 A. Alijagic, R. Russo and V. Scuderi, *et al.*, Sea urchin immune cells and associated microbiota co-exposed to iron oxide nanoparticles activate cellular and molecular reprogramming that promotes physiological adaptation, *J. Hazard. Mater.*, 2025, **485**, 136808, DOI: 10.1016/j.jhazmat.2024.136808.

22 M. Byrne, Annual reproductive cycles of the commercial sea urchin Paracentrotus lividus from an exposed intertidal and a sheltered subtidal habitat on the west coast of Ireland, *Mar. Biol.*, 1990, **104**(2), 275–289, DOI: 10.1007/BF01313269.

23 M. Guettaf, G. A. San Martin and P. Francour, Interpopulation variability of the reproductive cycle of Paracentrotus lividus (Echinodermata: Echinoidea) in the south-western Mediterranean, *J. Mar. Biol. Assoc. U. K.*, 2000, **80**(5), 899–907, DOI: 10.1017/S0025315400002885.

24 J. Lozano, J. Galera, S. Lopez, X. Turon and C. Palacin, Biological cycles and recruitment of Paracentrotus lividus (Echinodermata: Echinoidea) in two contrasting habitats, *Mar. Ecol.: Prog. Ser.*, 1995, **122**, 179–191, DOI: 10.3354/meps.

25 V. Matranga, A. Pinsino and M. Celi, *et al.*, Monitoring Chemical and Physical Stress Using Sea Urchin Immune Cells, in *Echinodermata*, ed. V. Matranga, Progress in Molecular and Subcellular Biology, Springer-Verlag, 2005, vol. 39, pp. 85–110, DOI: 10.1007/3-540-27683-1_5.

26 C. Falugi, M. G. Aluigi, M. C. Chiantore, D. Privitera, P. Ramoino, M. A. Gatti, A. Fabrizi, A. Pinsino and V. Matranga, Toxicity of metal oxide nanoparticles in immune cells of the sea urchin, *Mar. Environ. Res.*, 2012, **76**, 114–121, DOI: 10.1016/j.marenvres.2011.10.003.

27 P. Prosposito, L. Burratti and A. Bellingeri, Bifunctionalized Silver Nanoparticles as Hg2+ Plasmonic Sensor in Water: Synthesis, Characterizations, and Ecosafety, *Nanomaterials*, 2019, **9**(10), 1353, DOI: 10.3390/nano9101353.

28 M. P. Monopoli, A. S. Pitek, I. Lynch and K. A. Dawson, Formation and Characterization of the Nanoparticle–Protein Corona, in *Nanomaterial Interfaces in Biology*, Methods in Molecular Biology, ed. P. Bergese and K. Hamad-Schifferli, Humana Press, 2013, vol. 1025, pp. 137–155, DOI: 10.1007/978-1-62703-462-3_11.

29 A. Carpentieri, A. Sebastianelli and C. Melchiorre, *et al.*, Mass spectrometry based proteomics for the molecular

fingerprinting of Fiano, Greco and Falanghina cultivars, *Food Res. Int.*, 2019, **120**, 26–32, DOI: 10.1016/j.foodres.2019.02.020.

30 B. Ma, K. Zhang and C. Hendrie, *et al.*, PEAKS: powerful software for peptide de novo sequencing by tandem mass spectrometry, *Rapid Commun. Mass Spectrom.*, 2003, **17**(20), 2337–2342, DOI: 10.1002/rcm.1196.

31 F. Marlétaz, A. Couloux and J. Poulain, *et al.*, Analysis of the P. lividus sea urchin genome highlights contrasting trends of genomic and regulatory evolution in deuterostomes, *Cell Genomics*, 2023, **3**(4), 100295, DOI: 10.1016/j.xgen.2023.100295.

32 P. Jones, D. Binns and H. Y. Chang, *et al.*, InterProScan 5: genome-scale protein function classification, *Bioinformatics*, 2014, **30**(9), 1236–1240, DOI: 10.1093/bioinformatics/btu031.

33 A. Alexa and J. Rahnenführer, *Gene set enrichment analysis with topGO*, 2007.

34 B. Zybailov, A. L. Mosley, M. E. Sardiu, M. K. Coleman, L. Florens and M. P. Washburn, Statistical Analysis of Membrane Proteome Expression Changes in Saccharomyces c erevisiae, *J. Proteome Res.*, 2006, **5**(9), 2339–2347, DOI: 10.1021/pr060161n.

35 V. Matranga, R. Bonaventura and G. Di Bella, Hsp70 as a stress marker of sea urchin coelomocytes in short term cultures, *Cell. Mol. Biol.*, 2002, **48**(4), 345–349.

36 L. C. Smith, T. S. Hawley, J. H. Henson, A. J. Majeske, M. Oren and B. Rosental, Methods for collection, handling, and analysis of sea urchin coelomocytes, in *Methods in Cell Biology*, Elsevier, 2019, vol. 150, pp. 357–389, DOI: 10.1016/bs.mcb.2018.11.009.

37 A. Pinsino and V. Matranga, Sea urchin immune cells as sentinels of environmental stress, *Dev. Comp. Immunol.*, 2015, **49**(1), 198–205, DOI: 10.1016/j.dci.2014.11.013.

38 W. Strober, Trypan Blue Exclusion Test of Cell Viability, *Curr. Protoc. Immunol.*, 2015, **111**(1), A3.B.1–A3.B.3, DOI: 10.1002/0471142735.ima03bs111.

39 D. Lowe, V. Fossato and M. Depledge, Contaminant-induced lysosomal membrane damage in blood cells of mussels Mytilus galloprovincialis from the Venice Lagoon:an in vitro study, *Mar. Ecol.: Prog. Ser.*, 1995, **129**, 189–196, DOI: 10.3354/meps129189.

40 A. Bellingeri, A. Ale and T. Rusconi, *et al.*, Nanosilver Environmental Safety in Marine Organisms: Ecotoxicological Assessment of a Commercial Nano-Enabled Product vs an Eco-Design Formulation, *Toxics*, 2025, **13**(5), 338, DOI: 10.3390/toxics13050338.

41 A. Bellingeri, C. Battocchio, C. Faleri, G. Protano, I. Venditti and I. Corsi, Sensitivity of Hydra vulgaris to Nanosilver for Environmental Applications, *Toxics*, 2022, **10**(11), 695, DOI: 10.3390/toxics10110695.

42 A. Brunelli, G. Pojana, S. Callegaro and A. Marcomini, Agglomeration and sedimentation of titanium dioxide nanoparticles (n-TiO2) in synthetic and real waters, *J. Nanopart. Res.*, 2013, **15**(6), 1684, DOI: 10.1007/s11051-013-1684-4.

43 W. L. Oliani, F. H. Pusceddu and D. F. Parra, Silver-titanium polymeric nanocomposite non ecotoxic with bactericide activity, *Polym. Bull.*, 2022, **79**(12), 10949–10968, DOI: 10.1007/s00289-021-04036-7.

44 C. D. Walkey, J. B. Olsen, H. Guo, A. Emili and W. C. W. Chan, Nanoparticle Size and Surface Chemistry Determine Serum Protein Adsorption and Macrophage Uptake, *J. Am. Chem. Soc.*, 2012, **134**(4), 2139–2147, DOI: 10.1021/ja2084338.

45 S. Tenzer, D. Docter and J. Kuharev, *et al.*, Rapid formation of plasma protein corona critically affects nanoparticle pathophysiology, *Nat. Nanotechnol.*, 2013, **8**(10), 772–781, DOI: 10.1038/nnano.2013.181.

46 E. Morelli, E. Gabellieri, A. Bonomini, D. Tognotti, G. Grassi and I. Corsi, TiO2 nanoparticles in seawater: Aggregation and interactions with the green alga Dunaliella tertiolecta, *Ecotoxicol. Environ. Saf.*, 2018, **148**, 184–193, DOI: 10.1016/j.ecoenv.2017.10.024.

47 A. Alijagic, D. Gaglio and E. Napodano, *et al.*, Titanium dioxide nanoparticles temporarily influence the sea urchin immunological state suppressing inflammatory-relate gene transcription and boosting antioxidant metabolic activity, *J. Hazard. Mater.*, 2020, **384**, 121389, DOI: 10.1016/j.jhazmat.2019.121389.

48 L. E. González-García, M. N. MacGregor and R. M. Visalakshan, *et al.*, Nanoparticles Surface Chemistry Influence on Protein Corona Composition and Inflammatory Responses, *Nanomaterials*, 2022, **12**(4), 682, DOI: 10.3390/nano12040682.

49 A. A. Ashkarran, S. Tadjiki and Z. Lin, *et al.*, Protein Corona Composition of Gold Nanocatalysts, *ACS Pharmacol. Transl. Sci.*, 2024, **7**(4), 1169–1177, DOI: 10.1021/acsptsci.4c00028.

50 M. P. Monopoli, D. Walczyk and A. Campbell, *et al.*, Physical –Chemical Aspects of Protein Corona: Relevance to in Vitro and in Vivo Biological Impacts of Nanoparticles, *J. Am. Chem. Soc.*, 2011, **133**(8), 2525–2534, DOI: 10.1021/ja107583h.

51 W. Lai, Q. Wang, L. Li, Z. Hu, J. Chen and Q. Fang, Interaction of gold and silver nanoparticles with human plasma: Analysis of protein corona reveals specific binding patterns, *Colloids Surf., B*, 2017, **152**, 317–325, DOI: 10.1016/j.colsurfb.2017.01.037.

52 C. D. Walkey, J. B. Olsen and F. Song, *et al.*, Protein Corona Fingerprinting Predicts the Cellular Interaction of Gold and Silver Nanoparticles, *ACS Nano*, 2014, **8**(3), 2439–2455, DOI: 10.1021/nn406018q.

53 N. Durán, C. P. Silveira, M. Durán and D. Martinez, Silver nanoparticle protein corona and toxicity: a mini-review, *J. Nanobiotechnol.*, 2015, **13**, 55, DOI: 10.1186/s12951-015-0114-4.

54 I. Corsi, M. F. Desimone and J. Cazenave, Building the Bridge From Aquatic Nanotoxicology to Safety by Design Silver Nanoparticles, *Front. Bioeng. Biotechnol.*, 2022, **10**, 836742, DOI: 10.3389/fbioe.2022.836742.

55 M. C. Rex, A. Debroy, M. J. Nirmala and A. Mukherjee, Ecotoxicological significance of bio-corona formation on micro/nanoplastics in aquatic organisms, *RSC Adv.*, 2023, **13**(33), 22905–22917, DOI: 10.1039/D3RA04054B.

56 L. Canesi, C. Ciacci and R. Fabbri, *et al.*, Interactions of cationic polystyrene nanoparticles with marine bivalve hemocytes in a physiological environment: Role of soluble hemolymph proteins, *Environ. Res.*, 2016, **150**, 73–81, DOI: 10.1016/j.envres.2016.05.045.

57 L. Li, M. Stoiber and A. Wimmer, *et al.*, To What Extent Can Full-Scale Wastewater Treatment Plant Effluent Influence the Occurrence of Silver-Based Nanoparticles in Surface Waters?, *Environ. Sci. Technol.*, 2016, **50**(12), 6327–6333, DOI: 10.1021/acs.est.6b00694.

58 M. Al-Sid-Cheikh, S. J. Rowland, K. Stevenson, C. Rouleau, T. B. Henry and R. C. Thompson, Uptake, Whole-Body Distribution, and Depuration of Nanoplastics by the Scallop Pecten maximus at Environmentally Realistic Concentrations, *Environ. Sci. Technol.*, 2018, **52**(24), 14480–14486, DOI: 10.1021/acs.est.8b05266.

59 C. J. Dedman, A. M. King, J. A. Christie-Oleza and G. L. Davies, Environmentally relevant concentrations of titanium dioxide nanoparticles pose negligible risk to marine microbes, *Environ. Sci.: Nano*, 2021, **8**(5), 1236–1255, DOI: 10.1039/D0EN00883D.

60 Y. B. Hu, E. B. Dammer, R. J. Ren and G. Wang, The endosomal-lysosomal system: from acidification and cargo sorting to neurodegeneration, *Transl. Neurodegener.*, 2015, **4**(1), 18, DOI: 10.1186/s40035-015-0041-1.

61 L. Canesi, C. Ciacci, D. Vallotto, G. Gallo, A. Marcomini and G. Pojana, In vitro effects of suspensions of selected nanoparticles (C60 fullerene, TiO2, SiO2) on Mytilus hemocytes, *Aquat. Toxicol.*, 2010, **96**(2), 151–158, DOI: 10.1016/j.aquatox.2009.10.017.

62 E. Fröhlich, C. Meindl, E. Roblegg, B. Ebner, M. Absenger and T. R. Pieber, Action of polystyrene nanoparticles of different sizes on lysosomal function and integrity, *Part. Fibre Toxicol.*, 2012, **9**(1), 26, DOI: 10.1186/1743-8977-9-26.

63 M. N. Raghnaill, M. Bramini and D. Ye, *et al.*, Paracrine signalling of inflammatory cytokines from an in vitro blood brain barrier model upon exposure to polymeric nanoparticles, *Analyst*, 2014, **139**(5), 923–930, DOI: 10.1039/C3AN01621H.

64 F. Wang, L. Yu and M. P. Monopoli, *et al.*, The biomolecular corona is retained during nanoparticle uptake and protects the cells from the damage induced by cationic nanoparticles until degraded in the lysosomes, *Nanomed.: Nanotechnol., Biol. Med.*, 2013, **9**(8), 1159–1168, DOI: 10.1016/j.nano.2013.04.010.

65 S. Matthews, L. Mai, C. B. Jeong, J. S. Lee, E. Y. Zeng and E. G. Xu, Key mechanisms of micro- and nanoplastic (MNP) toxicity across taxonomic groups, *Comp. Biochem. Physiol., Part C: Toxicol. Pharmacol.*, 2021, **247**, 109056, DOI: 10.1016/j.cbpc.2021.109056.

66 A. E. Nel, L. Mädler and D. Velegol, *et al.*, Understanding biophysicochemical interactions at the nano–bio interface, *Nat. Mater.*, 2009, **8**(7), 543–557, DOI: 10.1038/nmat2442.

67 C. J. Coates, C. McCulloch, J. Betts and T. Whalley, Echinochrome A Release by Red Spherule Cells Is an Iron-Withholding Strategy of Sea Urchin Innate Immunity, *J. Innate Immun.*, 2018, **10**(2), 119–130, DOI: 10.1159/000484722.

68 A. Pinsino and A. Alijagic, Sea urchin Paracentrotus lividus immune cells in culture: formulation of the appropriate harvesting and culture media and maintenance conditions, *Biol. Open*, 2019, **8**, 3, DOI: 10.1242/bio.039289.

69 P. C. Branco, J. C. S. Borges, M. F. Santos, B. E. Jensch Junior and J. R. M. C. Da Silva, The impact of rising sea temperature on innate immune parameters in the tropical subtidal sea urchin Lytechinus variegatus and the intertidal sea urchin Echinometra lucunter, *Mar. Environ. Res.*, 2013, **92**, 95–101, DOI: 10.1016/j.marenvres.2013.09.005.

70 L. Stabili and P. Pagliara, The sea urchin Paracentrotus lividus immunological response to chemical pollution exposure: The case of lindane, *Chemosphere*, 2015, **134**, 60–66, DOI: 10.1016/j.chemosphere.2015.04.006.

71 V. Queiroz, V. Arizza, M. Vazzana and M. R. Custódio, Comparative evaluation of coelomocytes in Paracentrotus sea urchins: Description of new cell types and insights on spherulocyte maturation and sea urchin physiology, *Zool. Anz.*, 2022, **300**, 27–40, DOI: 10.1016/j.jcz.2022.06.008.

72 A. Bellingeri, N. Bono and I. Venditti, *et al.*, Capping drives the behavior, dissolution and (eco)toxicity of silver nanoparticles towards microorganisms and mammalian cells, *Environ. Sci.: Nano*, 2024, **11**(5), 2049–2060, DOI: 10.1039/D4EN00063C.

